

Learning A Coarse-to-Fine Diffusion Transformer for Image Restoration

Liyan Wang¹, Qinyu Yang¹, Cong Wang², Wei Wang³, Jinshan Pan⁴, Zhixun Su¹

¹Dalian University of Technology ²The Hong Kong Polytechnic University

³Sun Yat-sen University ⁴Nanjing University of Science and Technology

wangliyan@mail.dlut.edu.cn zxsu@dlut.edu.cn

Abstract

Recent years have witnessed the remarkable performance of diffusion models in various vision tasks. However, for image restoration that aims to recover clear images with sharper details from given degraded observations, diffusion-based methods may fail to recover promising results due to inaccurate noise estimation. Moreover, simple constraining noises cannot effectively learn complex degradation information, which subsequently hinders the model capacity. To solve the above problems, we propose a coarse-to-fine diffusion Transformer (C2F-DFT) for image restoration. Specifically, our C2F-DFT contains diffusion self-attention (DFSA) and diffusion feed-forward network (DFN) within a new coarse-to-fine training scheme. The DFSA and DFN respectively capture the long-range diffusion dependencies and learn hierarchy diffusion representation to facilitate better restoration. In the coarse training stage, our C2F-DFT estimates noises and then generates the final clean image by a sampling algorithm. To further improve the restoration quality, we propose a simple yet effective fine training scheme. It first exploits the coarse-trained diffusion model with fixed steps to generate restoration results, which then would be constrained with corresponding ground-truth ones to optimize the models to remedy the unsatisfactory results affected by inaccurate noise estimation. Extensive experiments show that C2F-DFT significantly outperforms diffusion-based restoration method IRSDE and achieves competitive performance compared with Transformer-based state-of-the-art methods on 3 tasks, including deraining, deblurring, and real denoising. The code is available at <https://github.com/wlydlut/C2F-DFT>.

Introduction

Image restoration aims to recover clean images from low-quality ones affected by various degradation factors, such as rain, noise, blur, and more. The need to restore high-quality images for post-processing vision applications has driven significant interest in image restoration research. Early conventional approaches in this field often rely on designing various statistical observations to properly formulate the problems (Dabov et al. 2007; Pan et al. 2016, 2017; Hu et al. 2014; Huang, Singh, and Ahuja 2015; Li et al. 2016). While these methods can achieve partial image recovery, they typically involve solving optimization algorithms that are challenging due to the non-convexity and non-smooth nature of the problems.



Figure 1: **Coarse training vs. fine training.** Unlike existing diffusion-based restoration models, e.g., (Valanarasu, Yasarla, and Patel 2022), which only constrain noises and obtain final restored results via a sampling algorithm (denoted as coarse training) that may fail to restore promising results due to inaccurate noise estimation, we propose the fine training to effectively improve restoration quality.

The advent of Convolutional Neural Networks (CNNs), capable of learning implicit priors from large-scale data, has led to the development of recent image restoration methods (Li et al. 2018; Ren et al. 2019; Kupyn et al. 2018, 2019; Tao et al. 2018; Guo et al. 2019; Wang et al. 2020b,a; Chen et al. 2021). However, CNNs have limitations due to their local receptive field and translation equivariance properties, which restrict their ability to model long-range pixel dependencies effectively. In contrast, Transformers (Dosovitskiy et al. 2021; Khan et al. 2021), with their attention mechanism that calculates responses at a given pixel through a weighted sum of all other positions, have emerged as a promising alternative. This attention design allows Transformers to capture long-range dependencies, making them powerful for image restoration tasks. Consequently, Transformers-based approaches have been successfully applied to image restoration tasks and achieved impressive performance (Wang et al. 2022; Zamir et al. 2022).

Recently, diffusion model (Ho, Jain, and Abbeel 2020) has garnered considerable attention for its powerful generative capability and remarkable performance across various vision tasks, such as image generation (Rombach et al. 2022; Song et al. 2021), inpainting (Xie et al. 2023), detection (Chen et al. 2022b), medical image segmentation (Rahman et al. 2023), and also image restoration (Choi et al. 2021; Saharia et al. 2023; Whang et al. 2022; Özdenizci

and Legenstein 2023; Luo et al. 2023). Unlike CNN and Transformer-based restoration methods that directly estimate final clear images from deep models, diffusion-based restoration models gradually recover clean images from noisy images generated in the forward diffusion process. However, we note these methods are often trained by constraining noises and then directly obtain final clean images by a sampling algorithm. This training approach limits the model capacity as the simple estimation of noises may introduce inaccuracies that subsequently affect the sampling restoration quality, as shown in Fig. 1.

To solve the above problems, we propose the C2F-DFT, a diffusion Transformer (DFT) with new coarse-to-fine (C2F) training scheme for image restoration. Specifically, the C2F-DFT is built with diffusion Transformer blocks that contain diffusion self-attention (DFSA) and diffusion feed-forward network (DFN), where the time step is embedded into DFSA and DFN, to respectively capture the long-range diffusion dependencies and learn hierarchy diffusion features to facilitate better restoration. To remedy the inaccuracy estimation of noise for restoration quality at the sampling process, we propose the coarse-to-fine training scheme. The coarse-to-fine training scheme contains (a) coarse training and (b) fine training. The coarse training is to train the diffusion Transformer by constraining noises, which would be exploited to obtain final restored images by a sampling algorithm. To further improve the restoration quality, we propose a simple yet effective fine training to further optimize the DFT by constraining the sampled restored images with corresponding ground truth ones instead of noises to avoid generating unsatisfactory results due to inaccurate noise estimation. With such designs, our fine training scheme can significantly improve the restoration quality compared with directly constraining noises in the coarse training, as shown in Fig. 1.

The main contributions are summarized as follows:

- We propose a diffusion Transformer for image restoration, which nicely embeds the diffusion into the Transformers, enabling it to not only model long-range dependencies but also fully exploit the generative ability of the diffusion model to facilitate better image restoration.
- We propose the coarse-to-fine training scheme to improve the restoration quality affected by the inaccurate noise estimation of diffusion models in coarse training, enabling to further scale up the model capacity in the fine training stage to facilitate better recovery.
- Extensive experiments show our C2F-DFT significantly outperforms recent diffusion-based method IR-SDE and achieves competitive performance compared with Transformer-based state-of-the-art methods on 3 tasks, including deraining, deblurring, and real denoising.

Diffusion Model Preliminaries

As one of the classic unconditional generation models, DDPM (Ho, Jain, and Abbeel 2020) provides basic theoretical support for subsequent unconditional diffusion and conditional diffusion. Specifically, the forward diffusion process follows the T steps Markov chain and gradually adds Gaussian noise according to a variance schedule

$\{\beta_1, \beta_2, \dots, \beta_T\}$ to the clean sample $\mathbf{x}_0 \sim q(\mathbf{x}_0)$. When T is large enough, \mathbf{x}_T is close to pure Gaussian noise. The process is:

$$\begin{aligned} q(\mathbf{x}_t | \mathbf{x}_{t-1}) &= \mathcal{N}(\mathbf{x}_t; \sqrt{1 - \beta_t} \mathbf{x}_{t-1}, \beta_t \mathbf{I}), \\ q(\mathbf{x}_{1:T} | \mathbf{x}_0) &= \prod_{t=1}^T q(\mathbf{x}_t | \mathbf{x}_{t-1}). \end{aligned} \quad (1)$$

where $t \sim \{0, \dots, T\}$; \mathbf{x}_t is the noise image at time step t .

Considering that the forward diffusion process admits sampling \mathbf{x}_t at an arbitrary timestep t in closed form,

$$q(\mathbf{x}_t | \mathbf{x}_0) = \mathcal{N}(\mathbf{x}_t; \sqrt{\bar{\alpha}_t} \mathbf{x}_0, (1 - \bar{\alpha}_t) \mathbf{I}), \quad (2)$$

where, $\alpha_t = 1 - \beta_t$, $\bar{\alpha}_t = \prod_{i=1}^t \alpha_i$. It should be noted that the training objective completely depends on Eq. (2). By using the reparameterization trick, we can sample some images \mathbf{x}_t at any time step t : $\mathbf{x}_t = \sqrt{\bar{\alpha}_t} \mathbf{x}_0 + \sqrt{1 - \bar{\alpha}_t} \epsilon_t$, where $\epsilon_t \sim \mathcal{N}(\mathbf{0}, \mathbf{I})$ has the same dimensionality as clean data \mathbf{x}_0 and latent variables \mathbf{x}_t .

In the reverse diffusion process, diffusion models are trained to learn the reverse process, that the joint distribution $p_\theta(\mathbf{x}_{0:T})$ defined by as a Markov chain with learned Gaussian transitions starting at $p(\mathbf{x}_T) = \mathcal{N}(\mathbf{x}_T; \mathbf{0}, \mathbf{I})$:

$$\begin{aligned} p_\theta(\mathbf{x}_{0:T}) &= p(\mathbf{x}_T) \prod_{t=1}^T p_\theta(\mathbf{x}_{t-1} | \mathbf{x}_t), \\ p_\theta(\mathbf{x}_{t-1} | \mathbf{x}_t) &= \mathcal{N}(\mathbf{x}_{t-1}; \mu_\theta(\mathbf{x}_t, t), \Sigma_\theta(\mathbf{x}_t, t)). \end{aligned} \quad (3)$$

Here, Ho, Jain, and Abbeel (2020) integrates $\mu_\theta(\mathbf{x}_t, t)$ reparameterize to noise prediction network $\epsilon_\theta(\mathbf{x}_t, t)$ with trainable model parameter θ :

$$\mu_\theta(\mathbf{x}_t, t) = \frac{1}{\sqrt{\bar{\alpha}_t}} (\mathbf{x}_t - \frac{1 - \bar{\alpha}_t}{\sqrt{1 - \bar{\alpha}_t}} \epsilon_\theta(\mathbf{x}_t, t)). \quad (4)$$

Because learning a diagonal variance Σ_θ leads to unstable training and poorer quality, Ho, Jain, and Abbeel (2020) adopts a simplified objective:

$$\begin{aligned} \mathcal{L}_t(\theta) &= \mathbb{E}_{t \sim [1, T], \mathbf{x}_0, \epsilon_t} [\|\epsilon_t - \epsilon_\theta(\mathbf{x}_t, t)\|^2] \\ &= \mathbb{E}_{t \sim [1, T], \mathbf{x}_0, \epsilon_t} [\|\epsilon_t - \epsilon_\theta(\sqrt{\bar{\alpha}_t} \mathbf{x}_0 + \sqrt{1 - \bar{\alpha}_t} \epsilon_t, t)\|^2]. \end{aligned} \quad (5)$$

Methodology

Our goal aims to effectively train the diffusion Transformer for better restoration. To that end, we propose a coarse-to-fine training pipeline to improve recovery quality.

Diffusion Transformer Model

Fig. 2 shows the overall of our diffusion Transformer (DFT), which is a 4-level U-shaped structure with diffusion Transformer blocks (DFTBs). The DFTBs consist of diffusion self-attention (DFSA) and diffusion feed-forward network (DFN), as shown in Fig. 2(a) and (b), respectively.

Overall Pipeline. Given the paired clean and degraded images $\{x, y\} \in \mathbb{R}^{H \times W \times 3}$, where $H \times W$ denotes the spatial dimension, we first obtain the noise sample $\mathbf{x}_t \in \mathbb{R}^{H \times W \times 3}$ by adding Gaussian noise $\epsilon_t \sim \mathcal{N}(\mathbf{0}, \mathbf{I})$ at time step t on

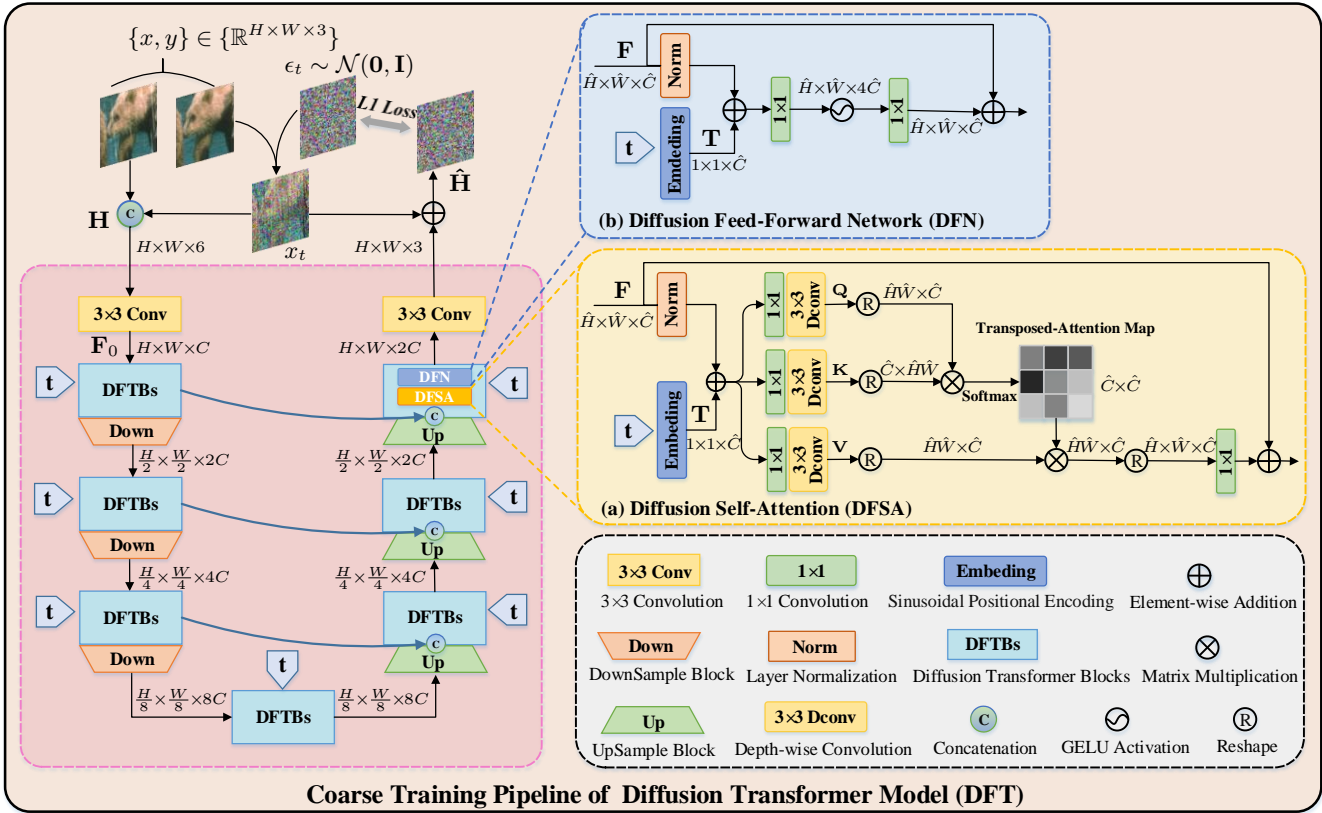


Figure 2: **Coarse Training Pipeline of Diffusion Transformer Model (DFT)**. We first add Gaussian noise to the clean image to obtain the noisy image according to the forward process of diffusion model (Ho, Jain, and Abbeel 2020) and concatenate it with the degraded images as the input of DFT. Then, the DFT is optimized by constraining the noise, and we can obtain the final clean images via a sampling algorithm. (a) Diffusion Self-Attention (DFSA) and (b) Diffusion Feed-Forward-Network (DFN) together build the diffusion Transformer block (DFTB), which respectively capture the long-range diffusion dependencies and learn hierarchy diffusion features to facilitate better restoration.

the clean image x according to the forward process of diffusion model (Ho, Jain, and Abbeel 2020), and concatenate x_t with the degraded image y at channel dimension to obtain $\mathbf{H} \in \mathbb{R}^{H \times W \times 6}$ as the input of DFT. Next, \mathbf{H} is encoded using a 3×3 convolution to obtain the embedding feature $\mathbf{F}_0 \in \mathbb{R}^{H \times W \times C}$, where C means the number of channel. \mathbf{F}_0 is hierarchically encoded and decoded via DFTBs, while the time t is encoded to the feature \mathbf{T} which is further embedded into the DFTBs. We also utilize skip connections to connect the features at the same level in the encoder and decoder. Finally, we use a 3×3 convolution to obtain the residual image, which is added to x_t to obtain the estimated noise $\hat{\mathbf{H}} \in \mathbb{R}^{H \times W \times 3}$.

Diffusion Self-Attention. Our DFSA aims to model long-range diffusion dependencies. Given the time step t of the diffusion model, we use sinusoidal positional encoding (Vaswani et al. 2017) to encode t into the vector embedding $\mathbf{T} \in \mathbb{R}^{1 \times 1 \times C}$ (as the dimension of time t is independent of image resolution, DFSA can process images with any sizes). We then embed the \mathbf{T} into given the input features \mathbf{F} to conduct self-attention (Zamir et al. 2022):

$$\begin{aligned} \text{DFSA}(\mathbf{F}, \mathbf{T}) &= \mathcal{A}(\mathbf{Q}, \mathbf{K}, \mathbf{V}) + \mathbf{F}, \\ \mathbf{Q}, \mathbf{K}, \mathbf{V} &= \text{Split}\left(W_d W_p(LN(\mathbf{F})) + \mathbf{T}\right), \end{aligned} \quad (6)$$

where W_p and W_d respectively denote 1×1 point-wise convolution and 3×3 depth-wise convolution; $\mathcal{A}(\mathbf{Q}, \mathbf{K}, \mathbf{V}) =$

$\mathbf{V} \cdot \text{Softmax}(\mathbf{K} \cdot \mathbf{Q} / \alpha)$; Here, α is a learnable scaling parameter to control the magnitude of the dot product of \mathbf{K} and \mathbf{Q} before applying the softmax function; Split denotes the split operation; $LN(\cdot)$ means layer normalization (Ba, Kiros, and Hinton 2016).

Diffusion Feed-Forward Network. Our DFN is to learn hierarchy diffusion representation, which is achieved by exploiting the two 1×1 point-wise convolutions as well as the time step embedding \mathbf{T} to further process the output features \mathbf{F} of DFSA:

$$DFN(\mathbf{F}, \mathbf{T}) = W_p \phi W_p(LN(\mathbf{F}) + \mathbf{T}) + \mathbf{F}, \quad (7)$$

where ϕ denotes the non-linear activation function GELU.

Coarse-to-Fine Training Pipeline for Restoration

Our coarse-to-fine training scheme contains (a) coarse training and (b) fine training. The coarse training aims to train the diffusion Transformer by constraining noises, which would be exploited to obtain final restored images by a sampling algorithm, while the fine training further optimizes the diffusion Transformer by constraining the sampled clean images with fixed steps in the coarse training and corresponding ground truth ones to scale up the model capacity for better recovery.

Coarse Training. Our coarse training is similar to the existing conditional diffusion model, which is to estimate the

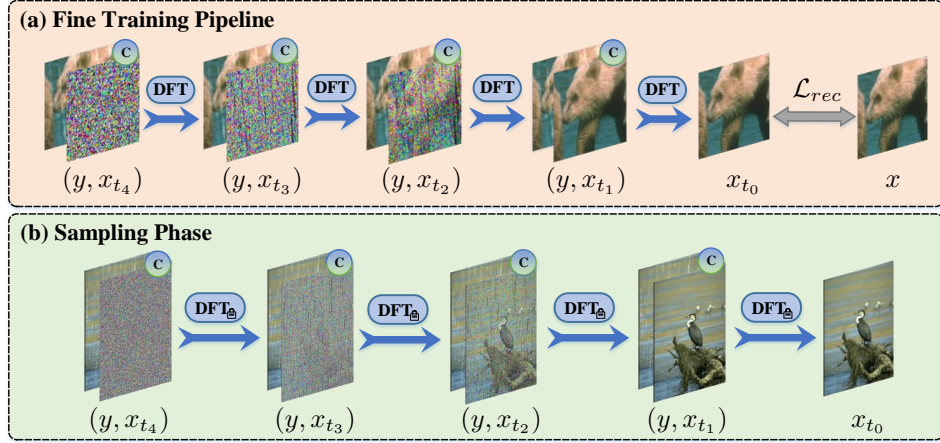


Figure 3: **(a) Fine Training Pipeline.** We first initialize the parameters of DFT with the well-trained parameters in the coarse training. We then adopt the sampling algorithm to generate clean images, which would participate in optimizing DFT by constraining the sampling restoration results with corresponding ground truth ones. **(b) Sampling Phase.** Our method can directly test the entire image with any size in a progressive restoration manner, greatly improving the restoration quality.

noise ϵ_t . Hence, the loss function in coarse training is:

$$\mathcal{L}_t(\theta) = \mathbb{E}_{t \sim [1, T], x_0, \epsilon_t} \|\epsilon_t - \epsilon_\theta(x_t, y, t)\|_1, \quad (8)$$

where the ϵ_θ denotes the noise estimation network, i.e., our diffusion Transformer in this paper. The estimated noise can be further exploited to produce final clean images via a sampling algorithm.

Fine Training. After completing the coarse training, we observe that 4-step sampling reaches the best restoration quality in terms of PSNR/SSIM, as shown in Tab. 4. However, as the coarse training primarily focuses on constraining noises, inaccurate noise estimation may significantly impact restoration quality (see Fig. 1 and 8). To address this problem to achieve better restoration, we propose a simple yet effective fine training scheme to further optimize the model by constraining the sampled restoration results with fixed sampling steps instead of noises, as shown in Fig. 3(a). The fine training stage has the same data processing as the coarse training but differs from the constraint objects. Specifically, we first initialize the parameters of DFT with the well-trained parameters from the coarse training. We then incorporate a sampling algorithm with 4-step to generate restoration results. Last, we optimize DFT by constraining the generated sampling restoration images with the corresponding ground-truth ones using L_1 loss (\mathcal{L}_1) and SSIM loss (\mathcal{L}_{ssim}) (Zhao et al. 2017) instead of constraining noise to remedy the unsatisfactory results in coarse training:

$$\mathcal{L}_{rec} = \lambda \mathcal{L}_{ssim}(x_{t_0}, x) + (1 - \lambda) \mathcal{L}_1(x_{t_0}, x), \quad (9)$$

where x_{t_0} denotes the generated sampled restoration results; $\mathcal{L}_{ssim}(x_{t_0}, x) = 1 - \text{SSIM}(x_{t_0}, x)$; λ is a weight.

We will demonstrate that the fine training phase has the capacity to surpass the performance limitations set by the diffusion model during the coarse training stage. This breakthrough not only paves the way for enhancing model capacity but also holds the potential to advance restoration tasks in future diffusion-based image restoration models.

Sampling Algorithm

During the sampling stage, we employ the implicit sampling strategy (Song, Meng, and Ermon 2021) to expedite

Algorithm 1: The sampling process of our C2F-DFT

Input: Degraded image y , diffusion Transformer $\epsilon_\theta(x_t, y, t)$, time steps T , implicit sampling steps S .

Output: Restored image x_{t_0} .

```

1:  $x_{t_s} \sim \mathcal{N}(0, \mathbf{I})$ 
2: for  $j = S, \dots, 1$  do
3:    $t_j = (j - 1) \cdot T / (S - 1) + 1$ 
4:    $t_{j-1} = (j - 2) \cdot T / (S - 1) + 1$  if  $j > 1$  else 0
5:    $\hat{\epsilon}_{t_j} = \epsilon_\theta(x_{t_j}, y, t_j)$ 
6:    $x_{t_{j-1}} = \sqrt{\bar{\alpha}_{t_{j-1}}} \left( \frac{x_{t_j} - \sqrt{1 - \bar{\alpha}_{t_j}} \cdot \hat{\epsilon}_{t_j}}{\sqrt{\bar{\alpha}_{t_j}}} \right) + \sqrt{1 - \bar{\alpha}_{t_{j-1}}} \cdot \hat{\epsilon}_{t_{j-1}}$ 
7: end for
8: return  $x_{t_0}$ 

```

our sampling process. The procedure for sampling within our C2F-DFT is outlined in Alg. 1. As we use the fine training scheme to train the DFT by constraining the sampled restoration results with corresponding ground truth ones instead of constraining noises, this advancement significantly enhances the quality of the samples. Fig. 3(b) shows our sampling outline, which progressively recovers clear images by the trained DFT.

Patch-Cycle Diffusion Learning Strategy

In contrast to existing diffusion models that rely on fixed patches for learning the diffusion process, we introduce a patch-cycle diffusion learning strategy, which enables diffusion models to capture more contextual information for better restoration. Specifically, we extract $p \times p$ patches from clean-degraded image pairs, denoted as $\{x^p, y^p\}$, where p is selected from $\{32, 64, 128\}$ in our experiments. During the training phase, we cyclically input $\{x^p, y^p\}_{p=32,64,128}$ into the C2F-DFT every N iterations and continue this training strategy until completion. To manage training costs, we decrease the batch size as p increases.

Experiments

We evaluate C2F-DFT on 3 popular image restoration tasks: **(a)** image deraining, **(b)** image deblurring, and **(c)** real im-

Methods	Test100		Rain100H		Rain100L		Test2800		Average		
	PSNR	SSIM	PSNR	SSIM	PSNR	SSIM	PSNR	SSIM	PSNR	SSIM	
CNN	RESCAN	25.00	0.835	26.36	0.786	29.80	0.881	31.29	0.904	28.11	0.851
	PreNet	24.81	0.851	26.77	0.858	32.44	0.950	31.75	0.916	28.94	0.893
	MSPFN	27.50	0.876	28.66	0.860	32.40	0.933	32.82	0.930	30.34	0.899
	MPRNet	30.27	0.897	30.41	0.890	36.40	0.965	33.64	0.938	32.68	0.922
	HINet	30.29	0.906	30.65	0.894	37.28	0.970	33.91	0.941	33.03	0.927
	SPAIR	30.35	0.909	30.95	0.892	36.93	0.969	33.34	0.936	32.89	0.926
TF	Restormer	32.00	0.923	<u>31.46</u>	<u>0.904</u>	<u>38.99</u>	<u>0.978</u>	34.18	0.944	34.15	<u>0.937</u>
DM	IR-SDE*	-	-	31.65*	0.904*	38.30*	0.980*	-	-	-	-
	IR-SDE	26.74	0.834	20.79	0.699	30.83	0.912	30.42	0.891	27.20	0.834
	C2F-DFT	31.38	0.921	31.62	0.909	39.03	0.980	34.03	0.944	34.01	0.938

Table 1: **Image deraining.** The CNN, TF, and DM respectively mean the CNN, Transformer, and diffusion model-based approaches. IR-SDE* denotes we use the provided pre-trained models to test, which respectively are individually trained on Rain100H and Rain100L. IR-SDE means we use the publicly available codes to re-train, where we train IR-SDE on Rain13K for fair comparisons, then test on different test sets. The **best** and second best are marked in bold and underlined, respectively.

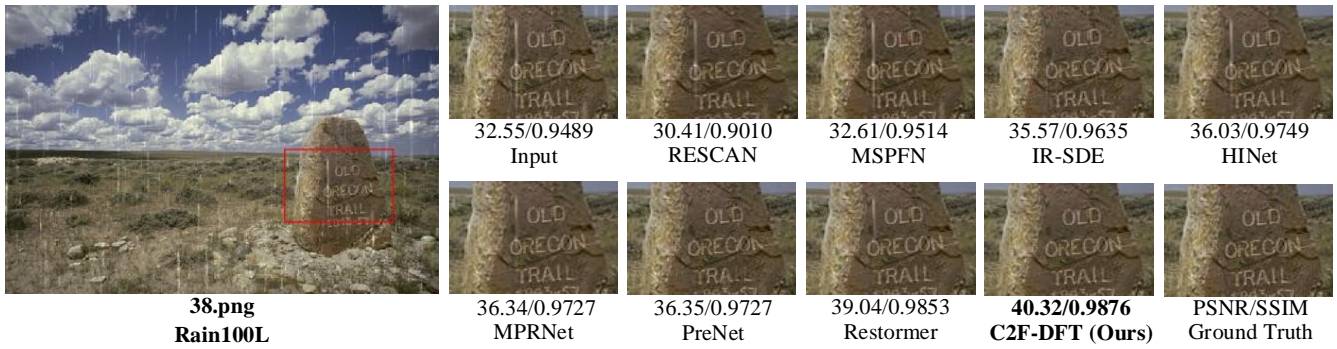


Figure 4: **Image deraining on Rain100L** (Yang et al. 2017). C2F-DFT is able to generate much cleaner results.

age denoising. More additional results and discussions are presented in supplementary materials.

Implementation Details

Network Settings. From level-1 to level-4, the number of DFTBs is [4, 6, 6, 8], attention heads in DFSA are [1, 2, 4, 8], and the number of channels is [48, 96, 192, 384].

Diffusion Settings. In diffusion training, we set the forward process variances to constants increasing linearly from $\beta_1 = 1e^{-4}$ to $\beta_2 = 2e^{-2}$, and the total time step T is set to 1000.

Coarse Training. We train our model using AdamW optimizer ($\beta_1=0.9$, $\beta_2=0.999$) with 270K iterations. We set the initial learning rate as $3e^{-4}$ which is gradually reduced to $1e^{-5}$ with the cosine annealing (Loshchilov and Hutter 2017). The (patch, batch) are cyclically updated by $[(32^2, 360), (64^2, 96), (128^2, 24)]$ at every 10K iterations.

Fine Training. After finishing the coarse training, we further train our model with 90K iterations with the initial learning rate $1e^{-5}$ gradually reduced to $1e^{-7}$ for fine image restoration. The (patch, batch) are cyclically updated by $[(32^2, 96), (64^2, 24), (128^2, 6)]$ at every 5K iterations. We empirically set $\lambda = 0.84$ in Eq. (9).

Main Results

Image Deraining. Similar to existing methods (Jiang et al. 2020; Zamir et al. 2021; Purohit et al. 2021; Zamir et al. 2022), we report PSNR/SSIM scores using Y channel in YCbCr color. Tab. 1 summarises quantitative comparisons, where our method consistently outperforms CNN-based methods, e.g., (Purohit et al. 2021), and is competitive with

Transformer-based methods (Zamir et al. 2022). Compared with diffusion model-based method IR-SDE (Luo et al. 2023), our method achieves a significant gain, increasing 6.81dB PSNR when averaged these benchmarks. Fig. 4 presents a visual example on Rain100L (Yang et al. 2017), where our C2F-DFT is able to recover a much clearer result.

Image Deblurring. Following (Zamir et al. 2022), we train our method on GoPro (Nah, Kim, and Lee 2017) and then directly applies to real benchmarks RealBlur-R and RealBlur-J (Rim et al. 2020). Tab. 2 shows that our method is slightly inferior to existing methods on the GoPro but shows a strong generalization to RealBlur datasets. It is worthy noticing that our method achieves the SOTA on RealBlur-R and is comparable with Restormer (Zamir et al. 2022) on RealBlur-J. Especially, our method significantly outperforms the diffusion model-based method IR-SDE (Luo et al. 2023) trained on GoPro by 4.69dB PSNR on RealBlur-J, demonstrating our method is a better diffusion deblurring model. Fig. 5 shows that our method is able to generate a sharper result with finer structures. These qualitative and quantitative results clearly show that our method is a strong deblurring diffusion model, especially on unseen scenes.

Real Image Denoising. Following (Zamir et al. 2022), our method is trained on SIDD (Abdelhamed, Lin, and Brown 2018) and then is directly applied to DND (Plötz and Roth 2017). Tab. 3 shows that our method is comparable with recent state-of-the-art NAFNet (Chen et al. 2022a) on SIDD, but outperforms it over 1.54dB on DND in terms of PSNR, which adequately illustrates our diffusion restoration method has a better generalization to unseen scenes,



Figure 5: **Image deblurring on RealBlur-R** (Rim et al. 2020). C2F-DFT is able to generate results with sharper structures.

Methods	GoPro		RealBlur-R		RealBlur-J		
	PSNR	SSIM	PSNR	SSIM	PSNR	SSIM	
CNN	DeblurGAN	28.70	0.858	33.79	0.903	27.97	0.834
	DeblurGAN-v2	29.55	0.934	35.26	0.944	28.70	0.866
	SRN	30.26	0.934	35.66	0.947	28.56	0.867
	DBGAN	31.10	0.942	33.78	0.909	24.93	0.745
	MT-RNN	31.15	0.945	35.79	0.951	28.44	0.862
	DMPHN	31.20	0.940	35.70	0.948	28.42	0.860
	SPAIR	32.06	0.953	-	-	28.81	0.875
	MIMO-UNet++	32.45	0.957	35.54	0.947	27.63	0.837
	MPRNet	32.66	0.959	35.99	0.952	28.70	0.873
	NAFNet	33.71	0.967	35.97	0.951	28.31	0.856
TF	Restormer	32.92	0.961	36.19	0.957	28.96	0.879
DM	IR-SDE	30.70	0.901	33.96	0.918	24.21	0.729
DM	C2F-DFT	31.96	0.928	36.34	0.957	28.90	0.876

Table 2: **Image deblurring.** Our method is trained on GoPro and then directly applies to RealBlur-R and RealBlur-J.

the same conclusion on image deblurring. We further provide a visual example on DND in Fig. 6, where our method has favorable denoising capability while preserving sharper structures by observing the locally enlarged areas.

Ablation Study

We conduct ablation study to verify the effectiveness of the proposed component on Rain100H test set.

Effect on Sampling Steps. Given that diffusion models involve sampling images iteratively until achieving satisfactory results, it becomes essential to analyze the impact of different sampling steps (denoted as S) on restoration quality. In Tab. 4, we present the distortion metrics PSNR/SSIM and the perception measurement LPIPS (Zhang et al. 2018), along with the corresponding sampling time. Notably, fewer sampling steps lead to higher distortion metrics (PSNR and SSIM), whereas more sampling steps yield improved perception results (LPIPS) at the cost of increased processing time. This observation aligns with the findings in (Whang et al. 2022). By carefully balancing these metrics and considering sampling time, we opt to utilize 4 sampling steps in constructing the fine training pipeline.

Effect on Patch-Cycle. We employ the patch-cycle training strategy to train our model, which raises questions about its effectiveness and impact on restoration quality. To address these concerns, we conduct separate training exper-

Methods	SIDD		DND		
	PSNR	SSIM	PSNR	SSIM	
CNN	CBDNet	30.78	0.801	38.06	0.942
	RIDNet	38.71	0.951	39.26	0.953
	AINDNet	39.08	0.954	39.37	0.951
	VDN	39.28	0.956	39.38	0.952
	DeamNet	39.47	0.957	39.63	0.953
	CycleISP	39.52	0.957	39.56	0.956
	MPRNet	39.71	0.958	39.80	0.954
	MIRNet	39.72	0.959	<u>39.88</u>	0.956
	NAFNet	40.30	0.961	38.41	0.943
	DM	C2F-DFT	39.84	0.960	39.95

Table 3: **Real image denoising.** Our method is trained on the SIDD training set and then is directly applied to DND.

S	PSNR \uparrow	SSIM \uparrow	LPIPS \downarrow	Time (s)
2	10.99	0.019	1.4166	31
3	25.61	0.878	0.1588	58
4	30.93	0.900	0.1313	102
5	30.44	0.894	0.1279	129
10	30.00	0.884	0.1231	237
25	29.30	0.868	0.1138	682
50	28.98	0.857	0.1092	818

Table 4: **Sampling steps S** for image restoration.

iments using patch-cycle and fixed patch approaches during the coarse training phase. The results in Tab. 5 demonstrate that our method outperforms fixed patch-based training while requiring a similar amount of training time.

Effect on Time Embedding. As we embed time step t into both DFSA and DFN in Transformers, one may wonder to know its effect on restoration. Tab. 6 shows that embedding t to Transformers can significantly improve the restoration quality by 4.08dB PSNR. The results reveal that time embedding is critical for diffusion-based image restoration methods. Fig. 7 shows that disabling t embedding hands down extensive noises, while embedding t to Transformers can significantly improve the visual restoration quality.

Effect on Coarse-to-Fine Training Strategy. We further analyze the effect on the proposed coarse-to-fine training pipeline. in Tab. 7. We also note that more iterations on coarse training only bring minor improvement (0.04dB in Tab. 7(a) vs. (b)). However, adding fine training on the completed coarse training can significantly improve the restora-

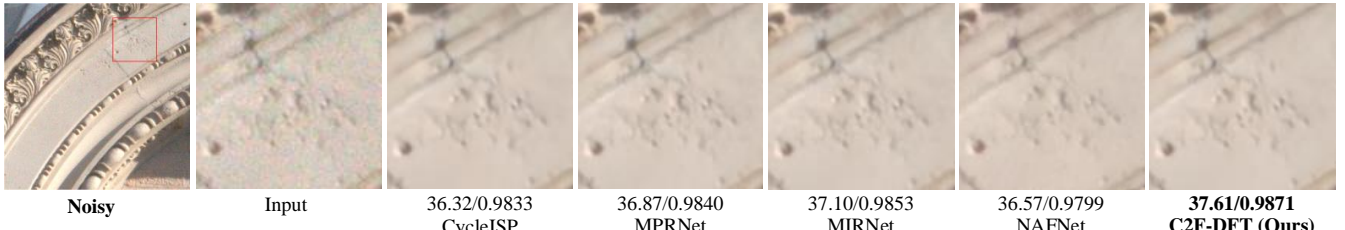


Figure 6: **Real image denoising on DND** (Plötz and Roth 2017). C2F-DFT produces cleaner results with finer details.

Training Patch	PSNR	SSIM	Training Time (h)
(a) Fixed Patch	30.52	0.896	84.2
(b) Patch-Cycle (Ours)	30.93	0.900	90.3

Table 5: **Fixed patch vs. patch-cycle** on diffusion training. For the fixed patch, we use the fixed 64×64 patch to train the diffusion model, while we use $\{32 \times 32, 64 \times 64, 128 \times 128\}$ patch to cyclically conduct the training process.

Experiment	PSNR	SSIM
(a) w/o t embedding	26.85	0.840
(b) w/ t embedding (Ours)	30.93	0.900

Table 6: **Without vs. with t embedding** effect on our DFT.



Figure 7: **Without vs. with t embedding** visual results. Disabling t embedding results in handing down extensive noises, while embedding t into Transformers can better remove noise and restore clearer images.

Training Iterations	PSNR	SSIM
(a) Coarse 270k (Tab. 5(b))	30.93	0.9000
(b) Coarse 360k	30.97	0.9001
(c) Coarse 270k + Fine 90k (Ours)	31.62	0.9094

Table 7: **Coarse-to-fine training pipeline** analysis.

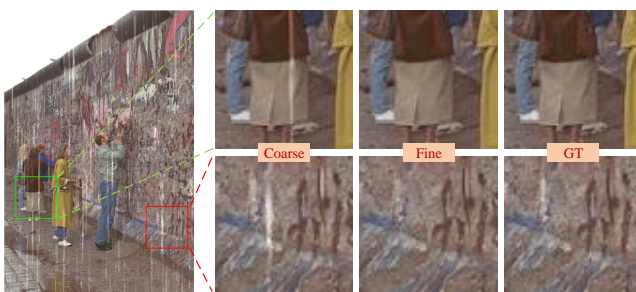


Figure 8: **Coarse vs. fine** visual results. Fine training is able to further produce clearer results with finer structures.

tion results, compared with the only coarse training versions (Tab. 7(c) vs. (a)-(b)). Fig. 1 and Fig. 8 show some examples on the comparisons between coarse and fine training, where our fine training significantly improves the visual restoration quality. This may be because using the fine training that constrains the sampled restored results with ground truth instead of noise to optimize the diffusion model can help the model learn more complex degraded information, which would fa-

cilitate the model to better restore clean images.

Related Work

We review image restoration methods and diffusion models.

Image Restoration. Traditional image restoration methods are mostly based on hand-crafted prior knowledge, such as sparse coding (Luo, Xu, and Ji 2015), self-similarity (Buades, Coll, and Morel 2005), gradient prior (Xu, Zheng, and Jia 2013), etc. With the emergence of Convolutional Neural Networks (Krizhevsky, Sutskever, and Hinton 2012; He et al. 2016), CNN-based image restoration methods (Park et al. 2020; Zhang et al. 2020, 2019; Anwar and Barnes 2019; Kim et al. 2020; Zamir et al. 2020a; Pathak et al. 2016; Zamir et al. 2020b) have achieved remarkable progress due to the powerful implicit learning ability from large-scale data. Recently, Transformer (Dosovitskiy et al. 2021) has been widely applied to image restoration due to learning the long dependencies between image patch sequences and capturing the global interaction information between contexts (Liang et al. 2021; Wang et al. 2022; Zamir et al. 2022). We refer the readers to the excellent literature review on image restoration (Anwar, Khan, and Barnes 2021; Li et al. 2019; Tian et al. 2020; Cho et al. 2021; Yue et al. 2019; Ren et al. 2021; Purohit et al. 2021), which summarise the main designs in deep image restoration models.

Diffusion Models. Recently, diffusion model (Ho, Jain, and Abbeel 2020) has achieved impressive performance due to its powerful generation ability. Inspired by conditional generation, conditional diffusion models have been widely used in image restoration, such as image super-resolution (Chung, Sim, and Ye 2022; Li et al. 2022; Luo et al. 2023), image repair (Esser et al. 2021; Jing et al. 2022), etc. Although these works have achieved better performance, these methods usually are constrained by noises, which limits the model capacity as the simple estimation of noises may introduce inaccuracies that subsequently affect the sampling restoration quality.

Conclusion

In this paper, we have proposed a diffusion Transformer with a new coarse-to-fine training scheme for image restoration. Observing that restoration quality may be affected due to inaccurate noise estimation in diffusion models, we have proposed the coarse-to-fine training scheme to improve the restoration quality by constraining the sampled restoration results instead of noises, enabling to facilitate better restoration in the fine training stage. Extensive experiments show that our C2F-DFT achieves competitive performance compared with state-of-the-art methods on 3 image restoration tasks, including deraining, deblurring, and real denoising.

References

Abdelhamed, A.; Lin, S.; and Brown, M. S. 2018. A high-quality denoising dataset for smartphone cameras. In *CVPR*, 1692–1700.

Anwar, S.; and Barnes, N. 2019. Real Image Denoising with Feature Attention. *ICCV*, 3155–3164.

Anwar, S.; Khan, S. H.; and Barnes, N. 2021. A Deep Journey into Super-resolution: A Survey. *ACM Comput. Surv.*, 53(3): 60:1–60:34.

Ba, J. L.; Kiros, J. R.; and Hinton, G. E. 2016. Layer normalization. *arXiv preprint. arXiv:1607.06450*.

Buades, A.; Coll, B.; and Morel, J. 2005. A Non-Local Algorithm for Image Denoising. In *CVPR*, 60–65.

Chen, L.; Chu, X.; Zhang, X.; and Sun, J. 2022a. Simple Baselines for Image Restoration. In *ECCV*, 17–33.

Chen, L.; Lu, X.; Zhang, J.; Chu, X.; and Chen, C. 2021. HINet: Half Instance Normalization Network for Image Restoration. In *CVPR*, 182–192.

Chen, S.; Sun, P.; Song, Y.; and Luo, P. 2022b. Diffusion-det: Diffusion model for object detection. *arXiv preprint. arXiv:2211.09788*.

Cho, S.-J.; Ji, S.-W.; Hong, J.-P.; Jung, S.-W.; and Ko, S.-J. 2021. Rethinking Coarse-to-Fine Approach in Single Image Deblurring. In *ICCV*, 4621–4630.

Choi, J.; Kim, S.; Jeong, Y.; Gwon, Y.; and Yoon, S. 2021. ILVR: Conditioning Method for Denoising Diffusion Probabilistic Models. In *ICCV*, 14347–14356.

Chung, H.; Sim, B.; and Ye, J. C. 2022. Come-Closer-Diffuse-Faster: Accelerating Conditional Diffusion Models for Inverse Problems through Stochastic Contraction. In *CVPR*, 12403–12412.

Dabov, K.; Foi, A.; Katkovnik, V.; and Egiazarian, K. 2007. Image denoising by sparse 3-D transform-domain collaborative filtering. *TIP*, 16(8): 2080–2095.

Dosovitskiy, A.; Beyer, L.; Kolesnikov, A.; Weissenborn, D.; Zhai, X.; Unterthiner, T.; Dehghani, M.; Minderer, M.; Heigold, G.; Gelly, S.; et al. 2021. An image is worth 16x16 words: Transformers for image recognition at scale. In *ICLR*.

Esser, P.; Rombach, R.; Blattmann, A.; and Ommer, B. 2021. ImageBART: Bidirectional Context with Multinomial Diffusion for Autoregressive Image Synthesis. In *NeurIPS*, 3518–3532.

Guo, S.; Yan, Z.; Zhang, K.; Zuo, W.; and Zhang, L. 2019. Toward convolutional blind denoising of real photographs. In *CVPR*, 1712–1722.

He, K.; Zhang, X.; Ren, S.; and Sun, J. 2016. Deep Residual Learning for Image Recognition. In *CVPR*, 770–778.

Ho, J.; Jain, A.; and Abbeel, P. 2020. Denoising Diffusion Probabilistic Models. In *NeurIPS*.

Hu, Z.; Cho, S.; Wang, J.; and Yang, M.-H. 2014. Deblurring Low-light Images with Light Streaks. In *CVPR*, 3382–3389.

Huang, J.-B.; Singh, A.; and Ahuja, N. 2015. Single Image Super-Resolution From Transformed Self-Exemplars. In *CVPR*, 5197–5206.

Jiang, K.; Wang, Z.; Yi, P.; Huang, B.; Luo, Y.; Ma, J.; and Jiang, J. 2020. Multi-Scale Progressive Fusion Network for Single Image Deraining. In *CVPR*, 8343–8352.

Jing, B.; Corso, G.; Berlinghieri, R.; and Jaakkola, T. S. 2022. Subspace Diffusion Generative Models. In *ECCV*, volume 13683, 274–289.

Khan, S.; Naseer, M.; Hayat, M.; Zamir, S. W.; Khan, F. S.; and Shah, M. 2021. Transformers in Vision: A Survey. *arXiv preprint. arXiv:2101.01169*.

Kim, Y.; Soh, J. W.; Park, G. Y.; and Cho, N. I. 2020. Transfer Learning from Synthetic to Real-Noise Denoising with Adaptive Instance Normalization. In *CVPR*, 3479–3489.

Krizhevsky, A.; Sutskever, I.; and Hinton, G. E. 2012. ImageNet Classification with Deep Convolutional Neural Networks. In *NIPS*, 1106–1114.

Kupyn, O.; Budzan, V.; Mykhailych, M.; Mishkin, D.; and Matas, J. 2018. DeblurGAN: Blind Motion Deblurring Using Conditional Adversarial Networks. In *CVPR*, 8183–8192.

Kupyn, O.; Martyniuk, T.; Wu, J.; and Wang, Z. 2019. DeblurGAN-v2: Deblurring (Orders-of-Magnitude) Faster and Better. In *ICCV*, 8877–8886.

Li, H.; Yang, Y.; Chang, M.; Chen, S.; Feng, H.; Xu, Z.; Li, Q.; and Chen, Y. 2022. SRDiff: Single image super-resolution with diffusion probabilistic models. *Neurocomputing*, 479: 47–59.

Li, S.; Araujo, I. B.; Ren, W.; Wang, Z.; Tokuda, E. K.; Junior, R. H.; Cesar-Junior, R.; Zhang, J.; Guo, X.; and Cao, X. 2019. Single image deraining: A comprehensive benchmark analysis. In *CVPR*, 3838–3847.

Li, X.; Wu, J.; Lin, Z.; Liu, H.; and Zha, H. 2018. Recurrent Squeeze-and-Excitation Context Aggregation Net for Single Image Deraining. In *ECCV*, volume 11211, 262–277.

Li, Y.; Tan, R. T.; Guo, X.; Lu, J.; and Brown, M. S. 2016. Rain streak removal using layer priors. In *CVPR*, 2736–2744.

Liang, J.; Cao, J.; Sun, G.; Zhang, K.; Van Gool, L.; and Timofte, R. 2021. SwinIR: Image restoration using swin transformer. In *ICCV Workshops*.

Loshchilov, I.; and Hutter, F. 2017. SGDR: Stochastic Gradient Descent with Warm Restarts. In *ICLR*.

Luo, Y.; Xu, Y.; and Ji, H. 2015. Removing Rain from a Single Image via Discriminative Sparse Coding. In *ICCV*, 3397–3405.

Luo, Z.; Gustafsson, F. K.; Zhao, Z.; Sjölund, J.; and Schön, T. B. 2023. Image Restoration with Mean-Reverting Stochastic Differential Equations. In *ICML*.

Nah, S.; Kim, T. H.; and Lee, K. M. 2017. Deep Multi-scale Convolutional Neural Network for Dynamic Scene Deblurring. In *CVPR*, 257–265.

Özdenizci, O.; and Legenstein, R. 2023. Restoring Vision in Adverse Weather Conditions With Patch-Based Denoising Diffusion Models. *TPAMI*, 45(8): 10346–10357.

Pan, J.; Hu, Z.; Su, Z.; and Yang, M.-H. 2017. L_0 -Regularized Intensity and Gradient Prior for Deblurring Text Images and Beyond. *TPAMI*, 39(2): 342–355.

Pan, J.; Sun, D.; Pfister, H.; and Yang, M.-H. 2016. Blind image deblurring using dark channel prior. In *CVPR*, 1628–1636.

Park, D.; Kang, D. U.; Kim, J.; and Chun, S. Y. 2020. Multi-Temporal Recurrent Neural Networks For Progressive Non-Uniform Single Image Deblurring With Incremental Temporal Training. In *ECCV*, volume 12351, 327–343.

Pathak, D.; Krahenbuhl, P.; Donahue, J.; Darrell, T.; and Efros, A. A. 2016. Context encoders: Feature learning by inpainting. In *CVPR*, 2536–2544.

Plötz, T.; and Roth, S. 2017. Benchmarking Denoising Algorithms with Real Photographs. In *CVPR*, 2750–2759.

Purohit, K.; Suin, M.; Rajagopalan, A.; and Boddeti, V. N. 2021. Spatially-Adaptive Image Restoration using Distortion-Guided Networks. In *ICCV*, 2289–2299.

Rahman, A.; Valanarasu, J. M. J.; Hacihamoglu, I.; and Patel, V. M. 2023. Ambiguous medical image segmentation using diffusion models. In *CVPR*, 11536–11546.

Ren, C.; He, X.; Wang, C.; and Zhao, Z. 2021. Adaptive Consistency Prior Based Deep Network for Image Denoising. In *CVPR*, 8596–8606.

Ren, D.; Zuo, W.; Hu, Q.; Zhu, P.; and Meng, D. 2019. Progressive Image Deraining Networks: A Better and Simpler Baseline. In *CVPR*, 3937–3946.

Rim, J.; Lee, H.; Won, J.; and Cho, S. 2020. Real-World Blur Dataset for Learning and Benchmarking Deblurring Algorithms. In *ECCV*, volume 12370, 184–201.

Rombach, R.; Blattmann, A.; Lorenz, D.; Esser, P.; and Ommer, B. 2022. High-Resolution Image Synthesis with Latent Diffusion Models. In *CVPR*, 10674–10685.

Saharia, C.; Ho, J.; Chan, W.; Salimans, T.; Fleet, D. J.; and Norouzi, M. 2023. Image Super-Resolution via Iterative Refinement. *TPAMI*, 45(4): 4713–4726.

Song, J.; Meng, C.; and Ermon, S. 2021. Denoising Diffusion Implicit Models. In *ICLR*.

Song, Y.; Sohl-Dickstein, J.; Kingma, D. P.; Kumar, A.; Ermon, S.; and Poole, B. 2021. Score-Based Generative Modeling through Stochastic Differential Equations. In *ICLR*.

Tao, X.; Gao, H.; Shen, X.; Wang, J.; and Jia, J. 2018. Scale-recurrent network for deep image deblurring. In *CVPR*, 8174–8182.

Tian, C.; Fei, L.; Zheng, W.; Xu, Y.; Zuo, W.; and Lin, C.-W. 2020. Deep learning on image denoising: An overview. *Neural Networks*, 131: 251–275.

Valanarasu, J. M. J.; Yasarla, R.; and Patel, V. M. 2022. Transweather: Transformer-based restoration of images degraded by adverse weather conditions. In *CVPR*, 2353–2363.

Vaswani, A.; Shazeer, N.; Parmar, N.; Uszkoreit, J.; Jones, L.; Gomez, A. N.; Kaiser, L.; and Polosukhin, I. 2017. Attention is All you Need. In *NeurIPS*, 5998–6008.

Wang, C.; Wu, Y.; Su, Z.; and Chen, J. 2020a. Joint Self-Attention and Scale-Aggregation for Self-Calibrated De-raining Network. In *ACM MM*, 2517–2525.

Wang, C.; Xing, X.; Wu, Y.; Su, Z.; and Chen, J. 2020b. DCSFN: Deep Cross-scale Fusion Network for Single Image Rain Removal. In *ACM MM*, 1643–1651.

Wang, Z.; Cun, X.; Bao, J.; Zhou, W.; Liu, J.; and Li, H. 2022. Uformer: A General U-Shaped Transformer for Image Restoration. In *CVPR*, 17683–17693.

Whang, J.; Delbracio, M.; Talebi, H.; Saharia, C.; Dimakis, A. G.; and Milanfar, P. 2022. Deblurring via Stochastic Refinement. In *CVPR*, 16272–16282.

Xie, S.; Zhang, Z.; Lin, Z.; Hinz, T.; and Zhang, K. 2023. SmartBrush: Text and Shape Guided Object Inpainting With Diffusion Model. In *CVPR*, 22428–22437.

Xu, L.; Zheng, S.; and Jia, J. 2013. Unnatural L0 Sparse Representation for Natural Image Deblurring. In *CVPR*, 1107–1114.

Yang, W.; Tan, R. T.; Feng, J.; Liu, J.; Guo, Z.; and Yan, S. 2017. Deep Joint Rain Detection and Removal from a Single Image. In *CVPR*, 1685–1694.

Yue, Z.; Yong, H.; Zhao, Q.; Meng, D.; and Zhang, L. 2019. Variational denoising network: Toward blind noise modeling and removal. In *NeurIPS*, 1688–1699.

Zamir, S. W.; Arora, A.; Khan, S.; Hayat, M.; Khan, F. S.; and Yang, M.-H. 2022. Restormer: Efficient Transformer for High-Resolution Image Restoration. In *CVPR*, 5718–5729.

Zamir, S. W.; Arora, A.; Khan, S.; Hayat, M.; Khan, F. S.; Yang, M.-H.; and Shao, L. 2021. Multi-Stage Progressive Image Restoration. In *CVPR*, 14821–14831.

Zamir, S. W.; Arora, A.; Khan, S. H.; Hayat, M.; Khan, F. S.; Yang, M.; and Shao, L. 2020a. CycleISP: Real Image Restoration via Improved Data Synthesis. In *CVPR*, 2693–2702.

Zamir, S. W.; Arora, A.; Khan, S. H.; Hayat, M.; Khan, F. S.; Yang, M.; and Shao, L. 2020b. Learning Enriched Features for Real Image Restoration and Enhancement. In *ECCV*, volume 12370, 492–511.

Zhang, H.; Dai, Y.; Li, H.; and Koniusz, P. 2019. Deep Stacked Hierarchical Multi-Patch Network for Image Deblurring. In *CVPR*, 5978–5986.

Zhang, K.; Luo, W.; Zhong, Y.; Ma, L.; Stenger, B.; Liu, W.; and Li, H. 2020. Deblurring by Realistic Blurring. In *CVPR*, 2734–2743.

Zhang, R.; Isola, P.; Efros, A. A.; Shechtman, E.; and Wang, O. 2018. The Unreasonable Effectiveness of Deep Features as a Perceptual Metric. In *CVPR*, 586–595.

Zhao, H.; Gallo, O.; Frosio, I.; and Kautz, J. 2017. Loss Functions for Image Restoration With Neural Networks. *TCI*, 3(1): 47–57.